Canadian Science Publishing | Transactions of the Canadian Society for Mechanical Engineering

Adaptive Wave Neural Network Nonsingular Terminal Sliding Mode Control for an Underwater Manipulator with Force Estimation

Journal:	*Transactions of the Canadian Society for Mechanical Engineering*
Manuscript ID	TCSME-2020-0010.R2
Manuscript Type:	Article
Date Submitted by the Author:	06-Apr-2020
Complete List of Authors:	Han, Lijun; Huazhong University of Science and Technology, school of naval architecture and ocean engineering Tang, Guoyuan; Huazhong University of Science and Technology, school of naval architecture and ocean engineering Zhou, Zengcheng; Huazhong University of Science and Technology, school of naval architecture and ocean engineering Huang, Hui; Huazhong University of Science and Technology, school of naval architecture and ocean engineering Xie, De; Huazhong University of Science and Technology, school of naval architecture and ocean engineering
Keywords:	adaptive wave neural network, nonsingular terminal sliding mode control, force estimation, path tracking, underwater manipulator
Is the invited manuscript for consideration in a Special Issue? :	Not applicable (regular submission)

Adaptive Wave Neural Network Nonsingular Terminal Sliding Mode Control for an Underwater Manipulator with Force Estimation

The first author: Lijun Han,

Affiliation:

1. School of Naval Architecture and Ocean Engineering, Huazhong University of Science and Technology, Wuhan, China

Corresponding author: Guoyuan Tang,

E-mail: tgyuan@hust.edu.cn

Affiliation:

1. School of Naval Architecture and Ocean Engineering, Huazhong University of Science and Technology, Wuhan, China

Co-author: Zengcheng Zhou,

Affiliation:

1. School of Naval Architecture and Ocean Engineering, Huazhong University of Science and Technology, Wuhan, China

Co-author: Hui Huang,

Affiliation:

1. School of Naval Architecture and Ocean Engineering, Huazhong University of Science and Technology, Wuhan, China

Co-author: De Xie,

Affiliation:

1. School of Naval Architecture and Ocean Engineering, Huazhong University of Science and Technology, Wuhan, China

Abstract

This paper proposes an adaptive wave neural network nonsingular terminal sliding mode control (AWNN-NTSMC) strategy with force estimation, which is exploited to address the path tracking control problem of the underwater manipulator under lumped disturbances. The proposed control scheme contains three parts: a nonsingular terminal sliding mode surface (NTSMS) part, an AWNN part and a force estimation part. The NTSMS is designed to make the system states achieve fast convergence in the sliding mode phase. The AWNN theory is utilized to approximate the lumped disturbances via on-line adjustment of the network parameters. The force estimation method is applied in compensating the effect of external force on the control system. Besides, a saturated function instead of the signum function is used aiming to the chattering suppression. Asymptotic stability of the closed-loop system is guaranteed by the Lyapunov stability. Finally, by using a six degree of freedom (DOF) underwater manipulator, comparative simulation results validate the better tracking performance and stronger robustness against disturbances of our proposed scheme.

Keywords: adaptive wave neural network, nonsingular terminal sliding mode control, force estimation, path tracking, underwater manipulator

1. Introduction

Space manipulators are widely applied in the field of aerospace, for the purpose of performing numerous maintenance and experiment tasks (Ellery 2008). Actually, they have certain extent flexibility due to the slender character of their links. Under some cases such as astronauts subjected to reaction force of the work object, the manipulator arms may suffer a large elastic deformation so that the astronauts would be moved for a distance in the direction of the reaction force, which is regarded as a protection method. Building a virtual scenario on the ground to support astronauts performing trainings has become an important means of enhancing the reliability and probability of success on space tasks. Another case that a large-scale underwater manipulator equipped in the surface water tank is to support trainers operation on the underwater weightless environment is commonly considered as an alternative to simulate space tasks. In addition, the flexible manipulator on the ground may easily appear the problems about the vibration (Kawamura et al. 2009) and instability and it is more difficult to control this kind of systems. To overcome these issues, this process can be transformed into the path tracking control problem that a rigid underwater manipulator end effector is subjected to external force instead of the flexible manipulator in the space, which is to simulate the displacement of space astronauts caused by the reaction force. Hence, to achieve this simulation requirement, some problems are necessary to be solved in advance. On the one hand, the exact model of the underwater manipulator is difficult to be established due to its nature of highly coupling and nonlinearity, and the effect of external disturbances like underwater currents, which can lead to the uncertainties of the system. In general, those external disturbances are mainly from workers and devices in the water tank. Another

problem is that the installation of force sensors is inconvenient in the underwater circumstances. Also, the reaction force that exerts on the manipulator end effector may have influence on the states of the manipulator system, i.e., leading to the changes of the position and velocity of its end effector. Therefore the control method is required to estimate the reaction force without force sensors.

To attenuate the effects of unknown disturbances, it can be found that recent years many methods for controlling the rigid manipulators have been proposed, mainly including PID control (Mohan and Kim 2015) and sliding mode control (SMC) (Jafarov et al. 2005; Mobayen 2015; Chu et al. 2017), etc. Compared with PID control, SMC methods are widely used owing to its fast convergence and good robustness against disturbances. It should be noted that the linear sliding surfaces (e.g., Jafarov et al. 2005) can only make the system errors realize asymptotic convergence, but nonlinear ones like terminal sliding mode control (TSMC) (e.g., Mobayen 2015) can reach the finite-time convergence. However, the existing singularity problem need be solved in Mobayen (2015). Recently, some nonsingular TSMC schemes (e.g., Song et al. 2016; Jin et al. 2017; Wang et al. 2016, 2019a, 2019b, 2019c, 2020; Qiao and Zhang 2019, 2020) have been reported and addressed such issues, owing to the modification of the sliding mode surfaces. Especially, the combination of TSMC method and integral theory has been used for the design of sliding mode surfaces in Qiao and Zhang (2019) and (2020). And, thanks to the advantage of fractional-order integrator and differentiator in comparison with integer-order ones, several fractional-order nonsingular TSMC manifolds (e.g., Wang et al. 2016, 2019b, 2019c, 2020) have been designed so that the control systems can obtain faster convergence and stronger robustness. Alternatively, an

adaptive dynamic global PID sliding mode strategy has been proposed (Chu et al. 2017), which has the global robustness in comparison with traditional SMC. Benefiting from Jin et al. (2017) and Chu et al. (2017), a modified NTSMS is proposed for the controller design in this paper. Since the upper bound of the uncertainties and disturbances is assumed to be known in Chu et al. (2017), it is more practical to consider the situation that the upper bound of the systematical uncertainties is unknown. In fact, this control problem under such condition has become a hot issue.

In such cases, adaptive network methods have been widely applied in the controller development, due to their powerful ability in estimating linear or nonlinear functions. More specifically, methods of the fuzzy and neural network (NN) are popular in the control design to compensate and estimate the lumped disturbances (Lin et al. 1998; Wai and Chen 2004; Rubio 2012; Vijay and Jena 2018). Among them, on-line training algorithm of a PI position controller was designed by Lin et al. (1998) via the fuzzy NN. Subsequently, a Takagi-Sugeno-Kang fuzzy NN method was proposed for the position control of a robot manipulator (Wai and Chen 2004). Besides, a modified optimal control strategy was proposed with the backpropagation network to address the tracking problem of robotic arms (Rubio 2012). Based on radial basis functional NN, the TSMC scheme combined with back-stepping techniques was considered to control a robot manipulator (Vijay and Jena 2018). By choosing appropriate learning algorithms to adjust the parameters online, the adaptive network methods can fully display their superiority, especially with the attachment of backpropagation learning algorithm (Lin et al. 1998; Rubio 2012) and the Lyapunov stability theory (Wai and Chen 2004; Vijay and Jena 2018). Another NN method such as

wave neural network (WNN) is efficient and popular in the control engineering in characterizing the local time-frequency features (Hsu et al. 2006 and Wei et al. 2012), compared with the conventional sigmoidal function NN. For example, the adaptive WNN approach combined with back-stepping techniques was proposed for a class of nonlinear systems (Hsu et al. 2006), while a robust WNN controller was designed to deal with the model uncertainties and disturbances (Rubio 2012). Undoubtedly, by comparison with traditional NN-based control systems, the learning ability and identification ability of the WNN controller can attain better control performance. Further, with the utilization of the SMC method and WNN, this paper considers the path tracking control of a fixed-base underwater manipulator against the parameter uncertainties and external disturbances.

Another problem is to observe the interaction force between the manipulator end effector and work object in order to guarantee the stability of the control system. In recent researches, some control algorithms instead of using force sensors have been used to estimate external force, where some restriction of force sensors like noise, dimensions of sensing can be eliminated. A common method to eliminate force sensors is applying disturbance observer (DO). In last two decades, many researchers have made the efforts in the applications of DO (Murakami et al. 1993; Katsura et al. 2006; Smith et al. 2006). Here, with the use of a DO, a force sensorless controller was proposed so as to achieve disturbance suppression and reaction force estimation (Murakami et al. 1993). Another method for the control system exerted on external force was designed by Katsura et al. (2006) based on a DO, which helped to relax the setting of the force bandwidth owing to the observer gain. In comparison with Murakami et al. (1993) and Katsura et al. (2006), Smith et al. (2006) proposed two

neural-network-based force/torque observers without requiring the information of the system dynamic model. However, a limitation for those methods is necessary to calculate the inverse of Jacobian transpose, which may cause some problems for the system near singular points. Another approach is employing an adaptive force estimator that can be utilized to compensate for the effect of external force using the adaptive law, without computing the inverse of Jacobian transpose (Danesh et al. 2005 and Dehghan et al. 2015). In addition, an adaptive controller with a force estimator was proposed (Danesh et al. 2005), where didn't involve in uncertainties of the control system. Depending on the regression matrix to deal with the parameter uncertainty, an AWNN control scheme (Dehghan et al. 2015) was designed by using the force estimation method. Subsequently, for object transportation of networked mobile manipulators, another AWNN control scheme without force/torque sensors was proposed by Ngo and Liu (2018), which also needed the regression matrix but cannot directly estimate the interactive force. It should be noted that solutions to the regression matrixes may cause excessive computation burden, especially for the system with three or more DOFs.

In this paper, an AWNN-NTSMC strategy with force estimation is proposed for the path tracking control of the underwater manipulator with the lumped disturbances, i.e., parameter uncertainties and external disturbances. Actually, a modified NTSMS is exploited in the controller development, which can guarantee the fast convergence and avoid the singularity condition. Afterwards, the AWNN method is utilized to approximate the lumped disturbances, in which the network parameters can be adjusted on-line based on the adaptive laws. Moreover, the force estimation method is introduced to compensate for the effect of external force that is exerted on the manipulator end effector. Note that the chattering

phenomenon occurs due to the high control gain in sliding mode control. To suppress the chattering, a saturated function of the dynamic boundary layer is considered to replace of the signum function. From considering the Lyapunov theory, the closed-loop system is proved to be asymptotical stability, which can guarantee its high-precision tracking performance and the strong robustness of disturbance rejection. Furthermore, simulations are carried out in several comparative cases to validate the control performance and effectiveness of the proposed controller. Then, some contributions can be described concisely in the following:

(1) A modified NTSMS has been proposed to achieve the fast convergence and avoid the singularity problem. (2) Thanks to the AWNN theory, the force estimation method and the boundary layer technique, the control scheme has been designed to compensate the effects of both the lumped disturbances and the external force on the system, and realize the chattering suppression. (3) According to the stability analysis, numerical simulations have been performed to demonstrate the better control performance of the proposed control scheme compared with several existing schemes.

This paper is organized as follows. At first, section 2 presents the control purpose, the kinematics and dynamics of the underwater manipulator. Section 3 describes an AWNN-NTSMC algorithm with force estimation, and analyses the stability of the system. In section 4, numerical simulation is performed on a 6-DOF underwater manipulator. Finally, the conclusions of this paper are summarized in section 5.

2. Problem description

Figure 1 describes that the rigid manipulator supports the trainer performing the tasks in

the three dimensional (3D) space. Figure 2 shows the motion of the manipulator end effector subjected to external force. If the flexible manipulator end effector is exerted on the reaction force $\boldsymbol{F}_{ext}$ of the work object at point C, its arms would appear a certain elastic deformation (see the dotted line ADE). Therefore, its end effector moves a distance in the direction of the reaction force $\boldsymbol{F}_{ext}$, i.e., from point C to point E. As shown in the introduction, the case that the flexible manipulator end effector shifts a distance due to the reaction force, can be replaced by the path tracking control for the rigid manipulator end effector. The latter way can greatly reduce the difficulty in the control process. That is, when the rigid manipulator end effector is exerted on the reaction force $\boldsymbol{F}_{ext}$, it can make its end effector move from point C to point E via the motion control for the manipulator. In this paper, the proposed control strategy can ensure the system stability and enhance the path control precision, while the force estimation method is utilized to compensate for the effect of the external force.

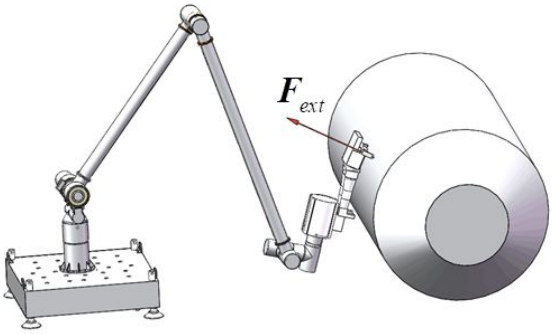

Fig. 1. The manipulator in 3D space

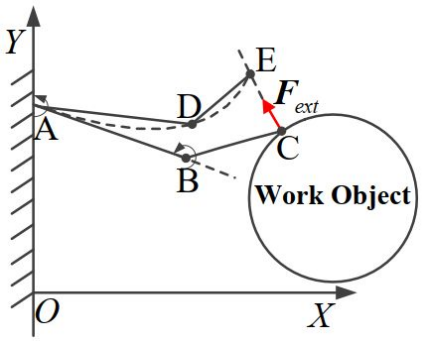

Fig. 2. The motion of the manipulator

Through the Lagrange function and the strip theory, the dynamic equation of the n DOF underwater manipulator is established and expressed in the following form:

$$\mathbf{M}(\boldsymbol{\theta})\ddot{\boldsymbol{\theta}}+\mathbf{C}(\boldsymbol{\theta},\dot{\boldsymbol{\theta}})\dot{\boldsymbol{\theta}}+\boldsymbol{G}(\boldsymbol{\theta})+\boldsymbol{\tau}_h+\boldsymbol{\tau}_d=\boldsymbol{\tau}+\mathbf{J}^{\mathrm{T}}\boldsymbol{F}_{ext} \tag{1}$$

where $\boldsymbol{\theta}$, $\dot{\boldsymbol{\theta}}$ and $\ddot{\boldsymbol{\theta}}\in\boldsymbol{R}^n$ denote the joint position vector, joint velocity vector, and joint acceleration vector, respectively. $\mathbf{M}(\boldsymbol{\theta})\in\mathbf{R}^{n\times n}$ is the symmetric positive definite inertial

matrix. $\mathbf{C}(\boldsymbol{\theta},\dot{\boldsymbol{\theta}}) \in \mathbf{R}^{n\times n}$ stands for the Coriolis and centrifugal matrix, and $\boldsymbol{G}(\boldsymbol{\theta}) \in \boldsymbol{R}^n$ is the gravitational vector. And, $(\dot{\mathbf{M}} - 2\mathbf{C})$ is skew symmetry (Wei et al. 2012) that meets $\boldsymbol{x}^{\mathrm{T}}(\dot{\mathbf{M}} - 2\mathbf{C})\boldsymbol{x} = 0$ for any vector $\boldsymbol{x} \in \boldsymbol{R}^n$. $\boldsymbol{\tau}_h \in \boldsymbol{R}^n$ represents the hydrodynamic torque vector including buoyancy, water resistance and additional mass force. $\boldsymbol{\tau}_d \in \boldsymbol{R}^n$ denotes the unknown disturbance torque vector and $\boldsymbol{\tau} \in \boldsymbol{R}^n$ is the joint input torque vector. Here only the parameter uncertainties and the external disturbance are considered and other factors like friction forces are ignored. $\mathbf{J} \in \mathbf{R}^{l\times n}$ denotes the Jacobian matrix from joint space to end effector position space. $\boldsymbol{F}_{ext} \in \boldsymbol{R}^l$ is the external force exerted on the manipulator end effector.

2.1 Wavelet neural network

1) Input layer transmits variables s_i $(i = 1,\mathrm{L}\ ,n)$ to the next layer, where s_i represents the elements of the sliding mode surface $\boldsymbol{s}$.

2) Membership layer represents the input values with the following wavelet basis function(Lin 2006):

$$\psi_i^j(s_i) = (1-((s_i - b_i^j)\cdot a_i^j)^2)\exp(-((s_i - b_i^j)\cdot a_i^j)^2/2) \tag{2}$$

where a_i^j, b_i^j $(i = 1,\mathrm{L}\ ,n\ , j = 1,\mathrm{L}\ ,m)$ are the dilation and translation parameters, respectively. For convenience, with the combination of the dilation and translation parameters of the basis functions, we can define the adjustable parameter vectors $\boldsymbol{a}$ and $\boldsymbol{b}$ with their component forms, i.e., $\boldsymbol{a} = [a_1^1,\mathrm{L}\ ,a_1^m,\mathrm{L}\ ,a_n^1,\mathrm{L}\ ,a_n^m]^{\mathrm{T}}$ and $\boldsymbol{b} = [b_1^1,\mathrm{L}\ ,b_1^m,\mathrm{L}\ ,b_n^1,\mathrm{L}\ ,b_n^m]^{\mathrm{T}} \in \boldsymbol{R}^{mn}$.

3) Layer three is the output layer, and notes in this layer represent output linguistic variables. According to Multi Resolution Analysis (MRA), any function can be estimated by

a linear combination of wavelets. Suppose that $\boldsymbol{f}=[f_1,\mathrm{L}\ ,f_n]^{\mathrm{T}}$ denotes the layer output

$$f_i(\boldsymbol{s})=\sum_{j=1}^{m}w_i^j\Psi^j(\boldsymbol{s})+\varepsilon_i \tag{3}$$

where $\Psi^j(\boldsymbol{s})(j=1,\mathrm{L}\ ,m)$ is the j th wavelet transform of the inputs with the expression:

$$\Psi^j(\boldsymbol{s})=\prod_{i=1}^{n}\psi_i^j(s_i) \tag{4}$$

and w_i^j is the output layer weight of the j th wavelet to the i th output.

Alternatively, eq. (3) can be rewritten in an equivalent vector form

$$\boldsymbol{f}=\mathbf{W}^{\mathrm{T}}\boldsymbol{\Psi}+\boldsymbol{\varepsilon} \tag{5}$$

where $\boldsymbol{\Psi}=[\Psi^1,\mathrm{L}\ ,\Psi^m]^{\mathrm{T}}$, $\boldsymbol{\varepsilon}=[\varepsilon_1,\mathrm{L}\ ,\varepsilon_n]^{\mathrm{T}}$, $\boldsymbol{f}=[f_1,\mathrm{L}\ ,f_n]^{\mathrm{T}}\in\boldsymbol{R}^n$ and the weight matrix is defined as

$$\mathbf{W}^{\mathrm{T}}=\begin{bmatrix} w_1^1 & \mathrm{L} & w_1^m \\ \mathrm{M} & \mathrm{O} & \mathrm{M} \\ w_n^1 & \mathrm{L} & w_n^m \end{bmatrix}\in\mathbf{R}^{n\times m} \tag{6}$$

where $\boldsymbol{w}_i=[w_i^1,\mathrm{L}\ ,w_i^m]^{\mathrm{T}}$, $i=1,\mathrm{L}\ ,n$.

2.2 Notations and lemmas

In the paper, some notations are defined: $\|\boldsymbol{\varphi}\|_1=\sum_{i=1}^{n}|\varphi_i|$, $\|\boldsymbol{\varphi}\|_2=\sqrt{\boldsymbol{\varphi}^{\mathrm{T}}\boldsymbol{\varphi}}$, $[\varphi_1^{\alpha_1}]=\mathrm{sign}(\varphi_1)|\varphi_1|^{\alpha_1}$, $[\boldsymbol{\varphi}^{\boldsymbol{\alpha}}]=[[\varphi_1^{\alpha_1}],\mathrm{L}\ ,[\varphi_n^{\alpha_n}]]^{\mathrm{T}}$, $[\boldsymbol{\varphi}^r]=[[\varphi_1^r],\mathrm{L}\ ,[\varphi_n^r]]^{\mathrm{T}}$ where $r\in R_+$, $\boldsymbol{\varphi}=[\varphi_1,\mathrm{L}\ ,\varphi_n]^{\mathrm{T}}\in\boldsymbol{R}^n$, $\boldsymbol{\alpha}=[\alpha_1,\mathrm{L}\ ,\alpha_n]^{\mathrm{T}}\in\boldsymbol{R}_+^n$.

Lemma 1(Bhat and Bernstein 2005): Let $\beta_1,\mathrm{L}\ ,\beta_k>0$, such that the polynomial $\phi^k+\beta_k\phi^{k-1}+\mathrm{L}\ +\beta_2\phi+\beta_1$ is Hurwitz. For the system $\dot{y}_1=y_2,\mathrm{L}\ ,\dot{y}_{k-1}=y_k,\dot{y}_k=u$, there exists $\vartheta\in(0,1)$ such that, for every $\eta\in(1-\vartheta,1)$, the origin is a globally finite-time-stable equilibrium under the linearized feedback control law $u=-\beta_1[y_1^{\eta_1}]-\mathrm{L}\ -\beta_k[y_k^{\eta_k}]$, satisfying $\eta_{i-1}=\eta_i\eta_{i+1}/(2\eta_{i+1}-\eta_i)$ with $\eta_{k+1}=1$ and $\eta_k=\eta$.

3. The design for controller

Let $\boldsymbol{\theta}_d$ be a second-order differentiable desired joint position vector, and define its joint position tracking error $\boldsymbol{\theta}_e$ and velocity tracking error $\dot{\boldsymbol{\theta}}_e$, i.e., $\boldsymbol{\theta}_e = \boldsymbol{\theta} - \boldsymbol{\theta}_d$ and $\dot{\boldsymbol{\theta}}_e = \dot{\boldsymbol{\theta}} - \dot{\boldsymbol{\theta}}_d$. The design objective of the controller is to ensure that the tracking position error $\boldsymbol{\theta}_e$ can achieve the asymptotic convergence to the equilibrium point.

3.1 NTSMC scheme

Motivated by the design of the sliding mode surface that can achieve fast convergence and avoid singularity, and inspired by Chu et al. (2017) and Jin et al. (2017), a modified NTSMC variable $\boldsymbol{s}$ is designed as

$$\boldsymbol{s} = \boldsymbol{s}_c + \mathbf{C}_3 \int_0^t [\boldsymbol{s}_c^{\boldsymbol{\alpha}_3}] dt \tag{7}$$

or equivalently written in the element form

$$s_i = s_{ci} + c_{3i} \int_0^t [s_{ci}^{\alpha_{3i}}] dt \tag{8}$$

and its auxiliary variable is

$$\boldsymbol{s}_c = \dot{\boldsymbol{\theta}}_e + \mathbf{C}_1 \int_0^t [\boldsymbol{\theta}_e^{\boldsymbol{\alpha}_1}] dt + \mathbf{C}_2 \int_0^t [\dot{\boldsymbol{\theta}}_e^{\boldsymbol{\alpha}_2}] dt - \boldsymbol{f}_s(t) \tag{9}$$

where $\boldsymbol{s} = [s_1, \cdots, s_n]^{\mathrm{T}}$ and $\boldsymbol{f}_s(t) = \boldsymbol{f}_s(0) e^{-\varphi t}$, satisfying $\boldsymbol{f}_s(0) = \dot{\boldsymbol{\theta}}_e(0) + c_0 \boldsymbol{\theta}_e(0)$ and the constant parameter $\varphi > 0$. And, these constant parameters like $\mathbf{C}_h = \mathrm{diag}[c_{h1}, \cdots, c_{hn}]$, $\boldsymbol{\alpha}_h = [\alpha_{h1}, \cdots, \alpha_{hn}]^{\mathrm{T}}$, $h = 1, 2, 3$ are selected according to the Lemma 1, satisfying $c_0, c_{1i}, c_{2i}, c_{3i} > 0$, $0 < \alpha_{1i}, \alpha_{3i} < 1$, $\alpha_{2i} = \alpha_{1i} / (2 - \alpha_{1i})$, $i = 1, \cdots, n$. In the sliding phase when $s_i(t) = 0$ $(i = 1, \cdots, n)$, its derivative can be expressed as $\dot{s}_{ci} + c_{3i}[s_{ci}^{\alpha_{3i}}] = 0$. Considering the case when $k = 1$ in Lemma 1: define another system $\dot{s}_{ci} = u$ with its control law $u = -c_{3i}[s_{ci}^{\alpha_{3i}}]$. By extending the above analysis to the cases of $i = 1, \cdots, n$, it can be concluded from Lemma 1 that the related variable $\boldsymbol{s}_c$ can realize the finite-time convergence under any

nonzero initial conditions. As with such situation, considering when $\boldsymbol{s}_c = \boldsymbol{0}$ in light of eq. (9) indicates that

$$\dot{\boldsymbol{\theta}}_e + \mathbf{C}_1 \int_0^t [\boldsymbol{\theta}_e^{\alpha_1}] dt + \mathbf{C}_2 \int_0^t [\dot{\boldsymbol{\theta}}_e^{\alpha_2}] dt - \boldsymbol{f}_s(t) = \boldsymbol{0} \tag{10}$$

and using the time derivative of eq. (10), it yields that the joint position tracking error can realize $\lim_{t\to\infty} \boldsymbol{\theta}_e = \boldsymbol{0}$ based on the theory of differential equation and Lemma 1.

In addition, define the following auxiliary variables

$$\dot{\boldsymbol{\theta}}_r = \dot{\boldsymbol{\theta}} - \boldsymbol{s} = \dot{\boldsymbol{\theta}}_d - \mathbf{C}_1 \int_0^t [\boldsymbol{\theta}_e^{\alpha_1}] dt - \mathbf{C}_2 \int_0^t [\dot{\boldsymbol{\theta}}_e^{\alpha_2}] dt + \boldsymbol{f}_s(t) \tag{11}$$

$$\ddot{\boldsymbol{\theta}}_r = \ddot{\boldsymbol{\theta}} - \dot{\boldsymbol{s}} = \ddot{\boldsymbol{\theta}}_d - (\mathbf{C}_1 [\boldsymbol{\theta}_e^{\alpha_1}] + \mathbf{C}_2 [\dot{\boldsymbol{\theta}}_e^{\alpha_2}]) + \dot{\boldsymbol{f}}_s(t) \tag{12}$$

Consider the system subjected to parameter uncertainties and external disturbance, and suppose that $\hat{\mathbf{M}}(\boldsymbol{\theta})$, $\hat{\mathbf{C}}(\boldsymbol{\theta}, \dot{\boldsymbol{\theta}})$, $\hat{\boldsymbol{G}}(\boldsymbol{\theta})$ and $\hat{\boldsymbol{\tau}}_h$ are nominal model parameters satisfying $\Delta\mathbf{M}(\boldsymbol{\theta}) = \mathbf{M}(\boldsymbol{\theta}) - \hat{\mathbf{M}}(\boldsymbol{\theta})$, $\Delta\mathbf{C}(\boldsymbol{\theta}, \dot{\boldsymbol{\theta}}) = \mathbf{C}(\boldsymbol{\theta}, \dot{\boldsymbol{\theta}}) - \hat{\mathbf{C}}(\boldsymbol{\theta}, \dot{\boldsymbol{\theta}})$, $\Delta\boldsymbol{G}(\boldsymbol{\theta}) = \boldsymbol{G}(\boldsymbol{\theta}) - \hat{\boldsymbol{G}}(\boldsymbol{\theta})$, $\Delta\boldsymbol{\tau}_h = \boldsymbol{\tau}_h - \hat{\boldsymbol{\tau}}_h$, where $\Delta\mathbf{M}(\boldsymbol{\theta})$, $\Delta\mathbf{C}(\boldsymbol{\theta}, \dot{\boldsymbol{\theta}})$, $\Delta\boldsymbol{G}(\boldsymbol{\theta})$, $\Delta\boldsymbol{\tau}_h$ are the model uncertainties. Define $\boldsymbol{f}$ as the lumped disturbance vector, namely $\boldsymbol{f} = -\Delta\mathbf{M}(\boldsymbol{\theta})\ddot{\boldsymbol{\theta}}_r - \Delta\mathbf{C}(\boldsymbol{\theta}, \dot{\boldsymbol{\theta}})\dot{\boldsymbol{\theta}}_r - \Delta\boldsymbol{G}(\boldsymbol{\theta}) - \Delta\boldsymbol{\tau}_h - \boldsymbol{\tau}_d$.

Theorem 1: Consider that the dynamic equation of the system is represented by eq. (1), and the lumped disturbance vector $\boldsymbol{f}$ is bounded as $\| \boldsymbol{f} \|_1 \le L_f$, where L_f is a known constant. Then, asymptotic stability of the whole system and boundness of the force estimation error can be guaranteed, if the system control law is designed as

$$\boldsymbol{\tau} = \hat{\mathbf{M}}(\boldsymbol{\theta})\ddot{\boldsymbol{\theta}}_r + \hat{\mathbf{C}}(\boldsymbol{\theta}, \dot{\boldsymbol{\theta}})\dot{\boldsymbol{\theta}}_r + \hat{\boldsymbol{G}}(\boldsymbol{\theta}) + \hat{\boldsymbol{\tau}}_h - \varepsilon_r \operatorname{sign}(\boldsymbol{s}) - \mathbf{J}^{\mathrm{T}} \hat{\boldsymbol{F}} \tag{13}$$

where $\varepsilon_r > L_f$, $\operatorname{sign}(\cdot)$ denotes signum function. $\hat{\boldsymbol{F}}$ is defined as the estimation of the external force $\boldsymbol{F}_{ext}$ and the adaptive law is updated as

$$\dot{\hat{\boldsymbol{F}}} = \mathbf{K}_F^{-\mathrm{T}} \mathbf{J} \boldsymbol{s} \tag{14}$$

where $\mathbf{K}_F$ is a positive definite and constant diagonal matrix.

Proof: Substituting eq. (13) into eq. (1) yields

$$\mathbf{M}\dot{\boldsymbol{s}} = \mathbf{M}(\ddot{\boldsymbol{\theta}} - \ddot{\boldsymbol{\theta}}_r) = \boldsymbol{f} - \mathbf{C}\boldsymbol{s} - \varepsilon_r \operatorname{sign}(\boldsymbol{s}) + \mathbf{J}^{\mathrm{T}}\tilde{\boldsymbol{F}} \tag{15}$$

where $\tilde{\boldsymbol{F}}$ denotes the force estimation error and satisfies $\tilde{\boldsymbol{F}} = \boldsymbol{F}_{ext} - \hat{\boldsymbol{F}}$.

Subsequently, choose a positive definite Lyapunov function as following:

$$V_1 = 1/2\boldsymbol{s}^{\mathrm{T}}\mathbf{M}\boldsymbol{s} + 1/2\tilde{\boldsymbol{F}}^{\mathrm{T}}\mathbf{K}_F\tilde{\boldsymbol{F}} \tag{16}$$

Taking the time derivative of eq. (16) along eqs. (14) and (15) results in

$$\begin{aligned}
\dot{V}_1 &= \boldsymbol{s}^{\mathrm{T}}\mathbf{M}\dot{\boldsymbol{s}} + 1/2\boldsymbol{s}^{\mathrm{T}}\dot{\mathbf{M}}\boldsymbol{s} + \tilde{\boldsymbol{F}}^{\mathrm{T}}\mathbf{K}_F\dot{\tilde{\boldsymbol{F}}} \\
&= \boldsymbol{s}^{\mathrm{T}}(\boldsymbol{f} - \mathbf{C}\boldsymbol{s} - \varepsilon_r \operatorname{sign}(\boldsymbol{s}) + \mathbf{J}^{\mathrm{T}}\tilde{\boldsymbol{F}}) + 1/2\boldsymbol{s}^{\mathrm{T}}\dot{\mathbf{M}}\boldsymbol{s} - \dot{\hat{\boldsymbol{F}}}^{\mathrm{T}}\mathbf{K}_F\tilde{\boldsymbol{F}} \\
&= \boldsymbol{s}^{\mathrm{T}}\boldsymbol{f} - \varepsilon_r \|\boldsymbol{s}\|_1 + (\boldsymbol{s}^{\mathrm{T}}\mathbf{J}^{\mathrm{T}} - \dot{\hat{\boldsymbol{F}}}^{\mathrm{T}}\mathbf{K}_F)\tilde{\boldsymbol{F}} \\
&\le -(\varepsilon_r - \|\boldsymbol{f}\|_1)\|\boldsymbol{s}\|_1
\end{aligned} \tag{17}$$

It can be deduced from the eq. (17) that V_1 is non-increasing and bounded function, so the boundness of the force estimation error can be obtained. In other words, we can conclude that the NTSMC variable $\lim_{t\to\infty} \boldsymbol{s} = \mathbf{0}$ according to the Barbalat's Lemma. Therefore, the joint position tracking error $\boldsymbol{\theta}_e$ can realize the asymptotic convergence by virtue of the designed NTSMC method.

3.2 AWNN-NTSMC scheme

Inspired from Wai and Muthusamy (2013) and Dehghan et al. (2015), we assume that the boundness of the lumped disturbance vector $\boldsymbol{f}$ is unknown. In this case, $\boldsymbol{f}$ is approached by the WNN scheme, with the combination of the proposed controller eq. (13) and update law eq. (14). By resorting to the approximation property of WNN scheme (Oussar et al., 1998), there exists the optimal parameters $\boldsymbol{a}^*$, $\boldsymbol{b}^*$, $\mathbf{W}^*$, such that

$$\boldsymbol{f} = \mathbf{W}^{*\mathrm{T}}\boldsymbol{\Psi}^*(\boldsymbol{s}, \boldsymbol{a}^*, \boldsymbol{b}^*) + \boldsymbol{\varepsilon} \tag{18}$$

where $\boldsymbol{\varepsilon}$ denotes the minimum approximation error. $\hat{\boldsymbol{f}}$ is the estimation of the vector $\boldsymbol{f}$,

which is defined as

$$\hat{\boldsymbol{f}} = \hat{\mathbf{W}}^{\mathrm{T}}\hat{\boldsymbol{\Psi}}(\boldsymbol{s},\hat{\boldsymbol{a}},\hat{\boldsymbol{b}}) \tag{19}$$

where $\hat{\boldsymbol{a}},\hat{\boldsymbol{b}},\hat{\mathbf{W}}$ represent the estimations of $\boldsymbol{a},\boldsymbol{b},\mathbf{W}$, respectively. In addition, the optimal parameters can be described as

$$(\boldsymbol{a}^*,\boldsymbol{b}^*,\mathbf{W}^*) = \underset{\hat{\boldsymbol{a}}\in\Omega_a,\hat{\boldsymbol{b}}\in\Omega_b,\hat{\boldsymbol{W}}\in\Omega_W}{\arg\min}\left\{\sup_{\boldsymbol{s}\in\Omega_s}\| \boldsymbol{f}-\hat{\mathbf{W}}^{\mathrm{T}}\hat{\boldsymbol{\Psi}}(\boldsymbol{s},\hat{\boldsymbol{a}},\hat{\boldsymbol{b}})\|_1\right\} \tag{20}$$

where $\Omega_a,\Omega_b,\Omega_{\mathrm{W}}$ are the proper bounded sets of $\boldsymbol{a},\boldsymbol{b},\mathbf{W}$ in WNN scheme, respectively.

Define the estimation error $\tilde{\boldsymbol{f}}$, and combining eqs. (18) and (19), we can obtain

$$\tilde{\boldsymbol{f}} = \boldsymbol{f}-\hat{\boldsymbol{f}} = \mathbf{W}^{*\mathrm{T}}\boldsymbol{\Psi}^* + \boldsymbol{\varepsilon} - \hat{\mathbf{W}}^{\mathrm{T}}\hat{\boldsymbol{\Psi}} = \tilde{\mathbf{W}}^{\mathrm{T}}\boldsymbol{\Psi}^* + \hat{\mathbf{W}}^{\mathrm{T}}\tilde{\boldsymbol{\Psi}} + \boldsymbol{\varepsilon} \tag{21}$$

where $\tilde{\mathbf{W}} = \mathbf{W}^* - \hat{\mathbf{W}}, \tilde{\boldsymbol{\Psi}} = \boldsymbol{\Psi}^* - \hat{\boldsymbol{\Psi}}$. In the controller development, we aim at adjusting the wavelet parameters with a proper adaptive law. Hence, linearization techniques, i.e., the Taylor series expansion is adopted to transform the nonlinear wavelet functions into the following linear form in partially

$$\begin{aligned}\tilde{\boldsymbol{\Psi}} &= [\frac{\partial \Psi^1}{\partial \boldsymbol{a}},\cdots,\frac{\partial \Psi^m}{\partial \boldsymbol{a}}]^{\mathrm{T}}|_{a=\hat{a}}(\boldsymbol{a}^*-\hat{\boldsymbol{a}}) + [\frac{\partial \Psi^1}{\partial \boldsymbol{b}},\cdots,\frac{\partial \Psi^m}{\partial \boldsymbol{b}}]^{\mathrm{T}}|_{b=\hat{b}}(\boldsymbol{b}^*-\hat{\boldsymbol{b}}) + \boldsymbol{o}_{ab} \\ &= \boldsymbol{\Psi}_a\tilde{\boldsymbol{a}} + \boldsymbol{\Psi}_b\tilde{\boldsymbol{b}} + \boldsymbol{o}_{ab}\end{aligned} \tag{22}$$

In terms of eq. (22), eq. (21) can be rewritten as

$$\begin{aligned}\tilde{\boldsymbol{f}} &= \tilde{\mathbf{W}}^{\mathrm{T}}\boldsymbol{\Psi}^* + \hat{\mathbf{W}}^{\mathrm{T}}\tilde{\boldsymbol{\Psi}} + \boldsymbol{\varepsilon} \\ &= \tilde{\mathbf{W}}^{\mathrm{T}}\hat{\boldsymbol{\Psi}} + \hat{\mathbf{W}}^{\mathrm{T}}\boldsymbol{\Psi}_a\tilde{\boldsymbol{a}} + \hat{\mathbf{W}}^{\mathrm{T}}\boldsymbol{\Psi}_b\tilde{\boldsymbol{b}} + \boldsymbol{\delta}\end{aligned} \tag{23}$$

with $\boldsymbol{\delta} = \mathbf{W}^{*\mathrm{T}}\boldsymbol{o}_{ab} + \tilde{\mathbf{W}}^{\mathrm{T}}\boldsymbol{\Psi}_a\tilde{\boldsymbol{a}} + \tilde{\mathbf{W}}^{\mathrm{T}}\boldsymbol{\Psi}_b\tilde{\boldsymbol{b}} + \boldsymbol{\varepsilon}$, satisfying $\|\boldsymbol{\delta}\|_1 \le \delta_r$. Denote $\hat{\delta}_r$ as the estimated value of δ_r, and its estimation error is $\tilde{\delta}_r = \delta_r - \hat{\delta}_r$.

Theorem 2: For the underwater manipulator system with the dynamic equation eq. (1) satisfying the unknown bounded assumption of the lumped disturbance term, if the update law of the force estimation is designed as eq. (14) and controller is formulated as eq. (24),

together with the parameter adaptive laws eqs. (25)-(27), then we have the following statements: (1) Asymptotic stability of the overall control system can be achieved, and the proposed controller ensures that the tracking errors tend to zero asymptotically; (2) The force estimation error $\tilde{\boldsymbol{F}}$ and parameter estimation errors in WNN scheme can be guaranteed to be bounded.

The control law in WNN scheme:

$$\boldsymbol{\tau}_{WNN} = \hat{\mathbf{M}}(\boldsymbol{\theta})\ddot{\boldsymbol{\theta}}_r + \hat{\mathbf{C}}(\boldsymbol{\theta},\dot{\boldsymbol{\theta}})\dot{\boldsymbol{\theta}}_r + \hat{\boldsymbol{G}}(\boldsymbol{\theta}) + \hat{\boldsymbol{\tau}}_h - \hat{\boldsymbol{f}} - \mathbf{K}_r\boldsymbol{s} - \hat{\delta}_r \operatorname{sign}(\boldsymbol{s}) - \mathbf{J}^{\mathrm{T}}\hat{\boldsymbol{F}} \quad (24)$$

and the parameter adaptive laws in WNN scheme

$$\dot{\hat{w}}_i = \eta_w \hat{\Psi} s_i, i = 1, \ldots, n \quad (25)$$

$$\dot{\hat{a}} = \eta_a \Psi_a^{\mathrm{T}} \hat{\mathbf{W}} \boldsymbol{s} \quad (26)$$

$$\dot{\hat{b}} = \eta_b \Psi_b^{\mathrm{T}} \hat{\mathbf{W}} \boldsymbol{s} \quad (27)$$

$$\dot{\hat{\delta}}_r = \eta_\delta \| \boldsymbol{s} \|_1 \quad (28)$$

Proof: Choose another positive definite Lyapunov function as following:

$$V_2 = 1/2\,\boldsymbol{s}^{\mathrm{T}}\mathbf{M}\boldsymbol{s} + (\tilde{a}\tilde{a})/(2\eta_a) + (\tilde{b}\tilde{b})/(2\eta_b) + \tilde{\delta}_r/(2\eta_\delta) + \operatorname{tr}(\tilde{\mathbf{W}}^{\mathrm{T}}\tilde{\mathbf{W}})/(2\eta_w) + 1/2\,\tilde{\boldsymbol{F}}^{\mathrm{T}}\mathbf{K}_F\tilde{\boldsymbol{F}} \quad (29)$$

where $\operatorname{tr}(\cdot)$ denotes the trace of a matrix.

Differentiating eq. (29) along eqs. (14), (24)-(28) gives

$$
\begin{aligned}
\dot{V}_2 &= \boldsymbol{s}^{\mathrm{T}}\mathbf{M}\dot{\boldsymbol{s}} + 1/2\boldsymbol{s}^{\mathrm{T}}\dot{\mathbf{M}}\boldsymbol{s} + (\dot{\tilde{\boldsymbol{a}}}^{\mathrm{T}}\tilde{\boldsymbol{a}})/\eta_a + (\dot{\tilde{\boldsymbol{b}}}^{\mathrm{T}}\tilde{\boldsymbol{b}})/\eta_b + \dot{\tilde{\delta}}_r\tilde{\delta}_r/\eta_\delta + \mathrm{tr}(\tilde{\mathbf{W}}^{\mathrm{T}}\dot{\tilde{\mathbf{W}}})/\eta_w + \dot{\tilde{\boldsymbol{F}}}^{\mathrm{T}}\mathbf{K}_F\tilde{\boldsymbol{F}} \\
&= \boldsymbol{s}^{\mathrm{T}}(\tilde{\boldsymbol{f}} - (\mathbf{C}+\mathbf{K}_r)\boldsymbol{s} - \hat{\delta}_r\mathrm{sign}(\boldsymbol{s}) + \mathbf{J}^{\mathrm{T}}\tilde{\boldsymbol{F}}) + 1/2\boldsymbol{s}^{\mathrm{T}}\dot{\mathbf{M}}\boldsymbol{s} + (\dot{\tilde{\boldsymbol{a}}}^{\mathrm{T}}\tilde{\boldsymbol{a}})/\eta_a + (\dot{\tilde{\boldsymbol{b}}}^{\mathrm{T}}\tilde{\boldsymbol{b}})/\eta_b + \cdots \\
&\quad + \dot{\tilde{\delta}}_r\tilde{\delta}_r/\eta_\delta + \mathrm{tr}(\tilde{\mathbf{W}}^{\mathrm{T}}\dot{\tilde{\mathbf{W}}})/\eta_w + \dot{\tilde{\boldsymbol{F}}}^{\mathrm{T}}\mathbf{K}_F\tilde{\boldsymbol{F}} \\
&= -\boldsymbol{s}^{\mathrm{T}}\mathbf{K}_r\boldsymbol{s} + \boldsymbol{s}^{\mathrm{T}}(\tilde{\mathbf{W}}^{\mathrm{T}}\hat{\boldsymbol{\Psi}} + \hat{\mathbf{W}}^{\mathrm{T}}\boldsymbol{\Psi}_a\tilde{\boldsymbol{a}} + \hat{\mathbf{W}}^{\mathrm{T}}\boldsymbol{\Psi}_b\tilde{\boldsymbol{b}} + \boldsymbol{\delta}) - \hat{\delta}_r\|\boldsymbol{s}\|_1 + (\dot{\tilde{\boldsymbol{a}}}^{\mathrm{T}}\tilde{\boldsymbol{a}})/\eta_a + \cdots \\
&\quad + (\dot{\tilde{\boldsymbol{b}}}^{\mathrm{T}}\tilde{\boldsymbol{b}})/\eta_b + \dot{\tilde{\delta}}_r\tilde{\delta}_r/\eta_\delta + \mathrm{tr}(\tilde{\mathbf{W}}^{\mathrm{T}}\dot{\tilde{\mathbf{W}}})/\eta_w + (\boldsymbol{s}^{\mathrm{T}}\mathbf{J}^{\mathrm{T}} - \dot{\tilde{\boldsymbol{F}}}^{\mathrm{T}}\mathbf{K}_F)\tilde{\boldsymbol{F}} \\
&= -\boldsymbol{s}^{\mathrm{T}}\mathbf{K}_r\boldsymbol{s} + \boldsymbol{s}^{\mathrm{T}}\boldsymbol{\delta} - \hat{\delta}_r\|\boldsymbol{s}\|_1 + (\boldsymbol{s}^{\mathrm{T}}\hat{\mathbf{W}}^{\mathrm{T}}\boldsymbol{\Psi}_a - \dot{\tilde{\boldsymbol{a}}}^{\mathrm{T}}/\eta_a)\tilde{\boldsymbol{a}} + (\boldsymbol{s}^{\mathrm{T}}\hat{\mathbf{W}}^{\mathrm{T}}\boldsymbol{\Psi}_b - \dot{\tilde{\boldsymbol{b}}}^{\mathrm{T}}/\eta_b)\tilde{\boldsymbol{b}} + \cdots \\
&\quad - \dot{\tilde{\delta}}_r\tilde{\delta}_r/\eta_\delta + \mathrm{tr}(\tilde{\mathbf{W}}^{\mathrm{T}}(\hat{\boldsymbol{\Psi}}\boldsymbol{s}^{\mathrm{T}} - \dot{\tilde{\mathbf{W}}}/\eta_w)) \\
&\le -\boldsymbol{s}^{\mathrm{T}}\mathbf{K}_r\boldsymbol{s} + \|\boldsymbol{s}\|_1\|\boldsymbol{\delta}\|_1 - \hat{\delta}_r\|\boldsymbol{s}\|_1 - \dot{\tilde{\delta}}_r\tilde{\delta}_r/\eta_\delta \\
&\le -\boldsymbol{s}^{\mathrm{T}}\mathbf{K}_r\boldsymbol{s} + \|\boldsymbol{s}\|_1\tilde{\delta}_r - \dot{\tilde{\delta}}_r\tilde{\delta}_r/\eta_\delta \\
&= -\boldsymbol{s}^{\mathrm{T}}\mathbf{K}_r\boldsymbol{s}
\end{aligned}
\tag{30}
$$

It can be deduced from the eq. (30) that $\dot{V}_2$ is negative semi-definite. According to the Lyapunov stability theory and Barbalat's Lemma, one can obtain that V_2 is bounded, and the NTSMC variable $\boldsymbol{s}$ can converge to zero asymptotically. Similar to the analysis of eq. (17), the joint position tracking error $\boldsymbol{\theta}_e$ can realize the asymptotic convergence with the proposed control strategy. Meanwhile, force estimation error $\tilde{\boldsymbol{F}}$ and parameter estimation errors $\tilde{\boldsymbol{a}}, \tilde{\boldsymbol{b}}, \tilde{\mathbf{W}}$ in WNN scheme can be guaranteed to be bounded.

Remark 1: According to the adaptive law in eq. (28), $\dot{\hat{\delta}}_r(t) \ge 0$ holds throughout the whole control process. Then, combining the positive gain η_δ and the asymptotical convergence of NTSMC variable $\boldsymbol{s}$, in practice, the value of $\hat{\delta}_r$ will keep a growing trend if the initial condition is set to satisfy $\hat{\delta}_r(0) \ge 0$, which may affect the stability of the system. To avoid the undesired issue and guarantee that the estimation $\hat{\delta}_r$ can be bounded, the adaptive law in eq. (28) is modified based on dead zones about the tracking error signal (Gao et al. 2017), by adding another damping term and being redefined as

$$
\dot{\hat{\delta}}_r = \begin{cases} \eta_\delta\|\boldsymbol{s}\|_1 - \xi_1\hat{\delta}_r, & for\ \|\boldsymbol{s}\|_1 > \gamma_1 \\ 0, & for\ \|\boldsymbol{s}\|_1 \le \gamma_1 \end{cases}
\tag{31}
$$

Remark 2: In order to attenuate the chattering phenomenon, here $\text{sign}(s_i)$ is replaced by $\text{sat}(s_i)$ in eq. (13) and eq. (24) to modify the proposed control law, where

$$\text{sat}(s_i) = \begin{cases} \tanh(s_i/\eta_{pi}), & for\ |s_i| < \eta_{pi} \\ \text{sign}(s_i), & for\ |s_i| \geq \eta_{pi} \end{cases} \tag{32}$$

In summary, the proposed controller can make the whole closed-loop system achieve the asymptotic stability. To make the control design more concise, Figs. 3-4 depict the control diagram of the underwater manipulator end effector tracking the desired path with the controller developed in section 3.1 and section 3.2, respectively. With the desired path in mind, the desired joint positions of the manipulator can be obtained via the inverse kinematics, and followed by the design of the NTSMS and the control law. Compared with Fig. 3, Fig. 4 takes advantage of the WNN scheme and adaptive laws to adjust the network relevant parameters in handling the lumped disturbances. Moreover, the force estimation method is introduced to estimate the external force exerted on the manipulator end effector. Based on the process formulated above, the full closed-loop system is formed. To this end, actual trajectory of the manipulator end effector can be acquired through the forward kinematics.

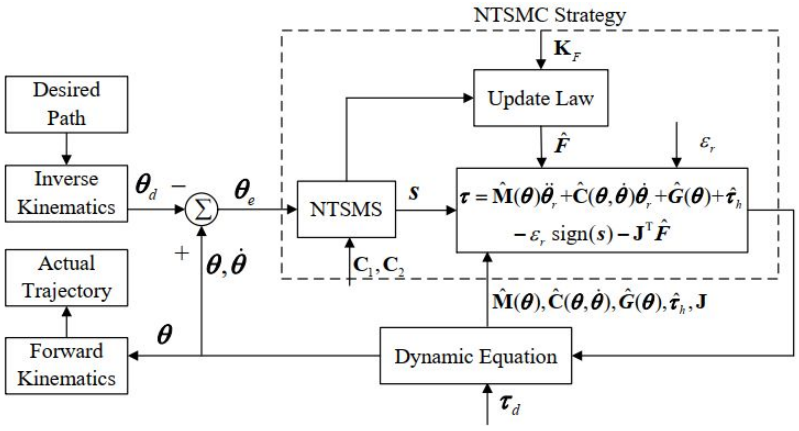

Fig. 3. The NTSMC diagram with force estimation

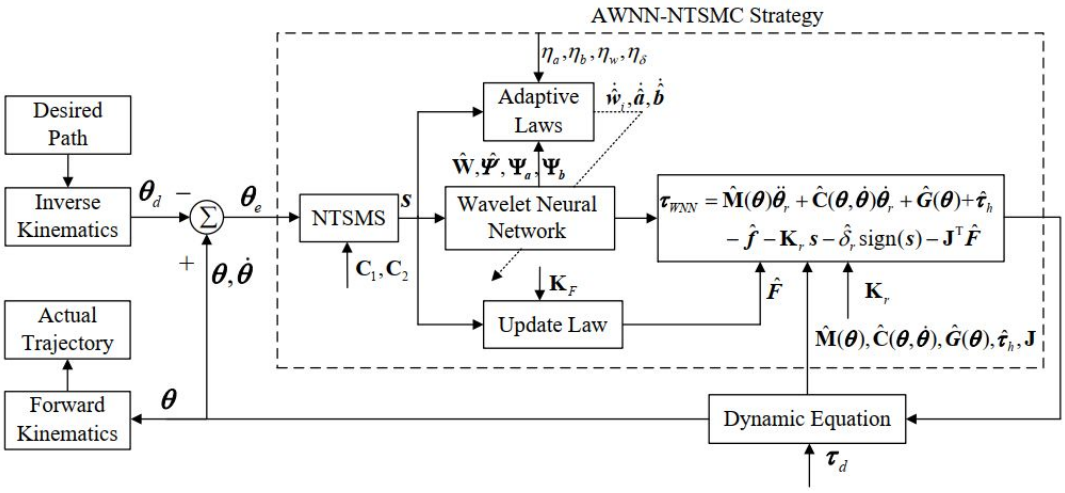

Fig. 4. The AWNN-NTSMC diagram with force estimation

4. Simulation

In order to testify the control performance of the proposed method, numerical simulations in MATLAB/Simulink environment are performed on a six DOF underwater manipulator. By use of the D-H notation, the link frames of this manipulator are established in Fig. 5, where four quantities are assigned in each link. They include joint variable θ_i, link twist α_{i-1}, link length a_{i-1} and link offset d_i, and their parameters values are detailed in Table 1. The link density of the manipulator is 2700kg/m^3. Assume that the centre of gravity is coincident with the centre of buoyancy, and the density of the fluid is 1025.9kg/m^3; the coefficients of both water resistance and additional mass force are $C_D = 1.05$ and $C_M = 0.8$, respectively. Consider that a complex desired path (X_d, Y_d, Z_d) is formulated as eq. (33) and starts from point A until to point I, shown in Fig. 6. The initial position of the manipulator end effector is (10.7105, 0, 0.7069) m, and the desired and actual orientation of the end effector are supposed to be the same.

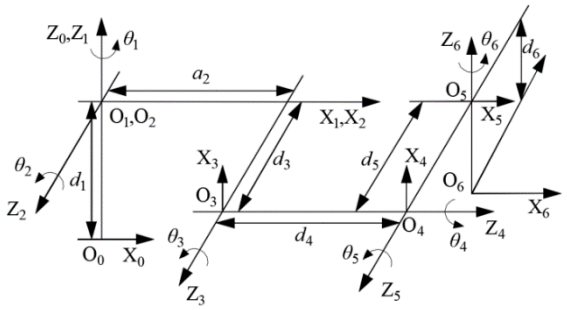

Fig. 5. The link frames of manipulator

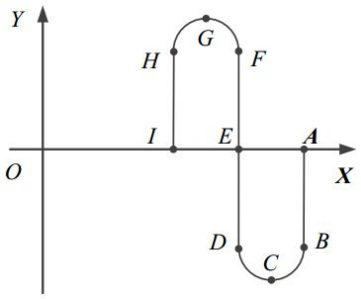

Fig. 6. Desired path ABCDEFGHI

Table 1. The link parameters of the manipulator

Parameter	Link 1	Link 2	Link 3	Link 4	Link 5	Link 6
$\alpha_{i-1}(^\circ)$	0°	90°	0°	90°	-90°	-90°
$a_{i-1}(\mathrm{m})$	0	0	5.0	0	0	0
$d_i(\mathrm{m})$	1.195	0	0.7	6.4	-0.7	-0.995
$\theta_i(^\circ)$	θ_1	θ_2	θ_3	θ_4	θ_5	θ_6

$$
\begin{aligned}
&\overline{\mathrm{AB}}: X_d = 10.72, -4 \le Y_d \le 0, Z_d = 1, (\mathrm{m}) \\
&\overline{\mathrm{BCD}}: 8.72 \le X_d \le 10.72, Y_d = -4 - \sqrt{1-(X_d-9.72)^2}, Z_d = 1, (\mathrm{m}) \\
&\overline{\mathrm{DEF}}: X_d = 8.72, -4 \le Y_d \le 4, Z_d = 1, (\mathrm{m}) \\
&\overline{\mathrm{FGH}}: 6.72 \le X_d \le 8.72, Y_d = 4 + \sqrt{1-(X_d-7.72)^2}, Z_d = 1, (\mathrm{m}) \\
&\overline{\mathrm{HI}}: X_d = 6.72, 0 \le Y_d \le 4, Z_d = 1, (\mathrm{m}).
\end{aligned} \tag{33}
$$

During the complex tracking process, simulations are performed under five cases and shown in the following:

Case 1: Only consider the bounded external disturbance and use the control method in section 3.1. Suppose $\boldsymbol{\tau}_d = [2,2,2,4,4,4]^{\mathrm{T}}\,\mathrm{N\,m}$ and external force $\boldsymbol{F}_{ext} = [40,50,0]^{\mathrm{T}}\,\mathrm{N}$ when $\mathrm{t} > 50\mathrm{s}$, and others are chosen as $\boldsymbol{\tau}_d = \boldsymbol{0}_{6\times1}\,\mathrm{N\,m}$ and $\boldsymbol{F}_{ext} = \boldsymbol{0}_{3\times1}\,\mathrm{N}$. In the control law $\varepsilon_r = 10$, and the parameter in the update law is $\boldsymbol{K}_F = diag\left[0.001, 0.001, 0.001\right]$.

Case 2-4: The system is subjected in the lumped disturbances and the external force, i.e., the nominal model parameters contain $\hat{\mathbf{M}}(\boldsymbol{\theta}) = 0.9\mathbf{M}(\boldsymbol{\theta})$, $\hat{\mathbf{C}}(\boldsymbol{\theta}, \dot{\boldsymbol{\theta}}) = 0.9\mathbf{C}(\boldsymbol{\theta}, \dot{\boldsymbol{\theta}})$, $\hat{\boldsymbol{G}}(\boldsymbol{\theta}) = \boldsymbol{G}(\boldsymbol{\theta})$,

$\hat{\boldsymbol{\tau}}_h = \boldsymbol{\tau}_h$; the external disturbance term is

$$\boldsymbol{\tau}_d = \begin{cases} \boldsymbol{0}_{6\times1}\,\text{N m}, & \text{for 0s} \le \text{t} \le \text{50s}, \\ [20,20,20,30,30,30]^{\text{T}}\,\text{N m}, & \text{for t} > \text{50s}, \end{cases} \tag{34}$$

and the external force is

$$\boldsymbol{F}_{ext} = \begin{cases} \boldsymbol{0}_{3\times1}\,\text{N}, & \text{for 0s} \le \text{t} \le \text{50s}, \\ [50\sin(0.1\text{t}), 30\cos(0.1\text{t}), 40\sin(0.1\text{t})]^{\text{T}}\,\text{N}, & \text{for t} > \text{50s}. \end{cases} \tag{35}$$

Case 5: Considering the system under the presence of the lumped disturbances and the external force, where the nominal model parameters consist of $\hat{\mathbf{M}}(\boldsymbol{\theta}) = 0.9\mathbf{M}(\boldsymbol{\theta})$, $\hat{\mathbf{C}}(\boldsymbol{\theta}, \dot{\boldsymbol{\theta}}) = 0.9\mathbf{C}(\boldsymbol{\theta}, \dot{\boldsymbol{\theta}})$, $\hat{\boldsymbol{G}}(\boldsymbol{\theta}) = 0.99\boldsymbol{G}(\boldsymbol{\theta})$, $\hat{\boldsymbol{\tau}}_h = 0.99\boldsymbol{\tau}_h$; both of the external disturbance and the external force are assumed the same as in case 4.

To clarify the better tracking performance of the proposed controller, comparisons are made with some advanced SMC strategies such as global PID-SMC (Chu et al. 2017) and NTSMC (Jin et al. 2017) for the system control. The designs of global PID-SMC and NTSMC are described separately as:

$$\text{(Case 2)}\ \boldsymbol{s}_1 = \dot{\boldsymbol{\theta}}_e + \mathbf{C}_1\int_0^t \boldsymbol{\theta}_e dt + \mathbf{C}_2\boldsymbol{\theta}_e - \boldsymbol{f}_s(t) \tag{36}$$

$$\text{(Case 3)}\ \boldsymbol{s}_2 = \dot{\boldsymbol{\theta}}_e + \mathbf{C}_1\int_0^t [\boldsymbol{\theta}_e^{\alpha_1}]dt + \mathbf{C}_2\int_0^t [\dot{\boldsymbol{\theta}}_e^{\alpha_2}]dt \tag{37}$$

where $\boldsymbol{f}_s(t)$ is chosen the same as the term in eq. (9). And, integrating the two sliding mode surfaces (eqs. (36)-(37)) with the adaptive laws (eqs. (25)-(27), (31)) and the control law (eqs. (24), (32)), two new strategies are obtained and compared with the proposed method that is considered as the fourth case. For case 5, its control parameters under the proposed scheme are chosen as same as ones in case 4, except for their different nominal model parameters including the gravitational and hydrodynamic terms. The parameter values of these four methods are assigned in Table 2. Here, five wavelet functions are adopted, and the

initialization of their parameters in the adaptive laws are set as $a_i^j(0) \in [0,1]$, $b_i^j(0) = 0.2$, $w_i^j(0) = 0.2$ $(i = 1,\cdots,6, j = 1,\cdots,5)$, $\hat{\delta}_r(0) = 0$. For the force estimation, let $\hat{\boldsymbol{F}}(0) = \boldsymbol{0}_{3\times1}$ N be its initial value. The total simulation time is 1000s, and its sampling time is 0.05s. Besides, the averaged position tracking errors E_x, E_y, E_z in three directions and their averaged total position error E_t, and the averaged force estimation error E_f are defined in the following:

$$E_x = \sqrt{\|\boldsymbol{e}_x\|_2^2 / N}, E_y = \sqrt{\|\boldsymbol{e}_y\|_2^2 / N}, E_z = \sqrt{\|\boldsymbol{e}_z\|_2^2 / N}, E_t = \sqrt{E_x^2 + E_y^2 + E_z^2} \quad (38)$$

$$E_f = \sqrt{\| \boldsymbol{F} - \hat{\boldsymbol{F}} \|_2^2 / N} \quad (39)$$

where $\boldsymbol{e}_x$, $\boldsymbol{e}_y$, $\boldsymbol{e}_z$ denotes separately the X, Y, Z direction position error vector, and N is the number of simulation steps.

Table 2. The parameters of the controllers

Terms	Parameters	Values
Sliding mode surface	$c_{1i}, c_{2i}, \alpha_{1i}, c_{3i}, \alpha_{3i}, c_0, \varphi$	9,6,0.9, 2,0.8,0.01,1
Wave neural network	$\eta_w, \eta_a, \eta_b, \eta_\delta, \xi_1, \gamma_1$	20,0.02,0.01,0.2,0.5,0.03
Force estimation	$\mathbf{K}_f$	diag[0.006, 0.004, 0.006]
Control law	$\mathbf{K}_r, \eta_{pi}$	30,0.1

For case 1, during the complex path tracking control of the underwater manipulator end effector, variations in the space positions and their corresponding errors in X, Y and Z direction are depicted in Figs. 7-10, respectively. It can be seen that, their three position errors can converge fast and reach small ranges at about 10s. However, the position of the manipulator end effector changes abruptly within a permitted range at 50s due to the sudden appearance of external disturbance and external force. Owing to the compensation for the external factors in section 3.1, after about 20s the manipulator end effector can still keep the

high-precision tracking control for the desired path. For example, their total position error can finally reach the range of [0, 0.005] m (see Fig. 11). Figure 12 illustrates the results of the components of external force and their estimations in three directions. Their estimation errors have few differences at the beginning except for the sudden changes at about 50s, and after that they become decreasing till within small regions. These results conclude that the control system in section 3.1 has fast convergence, good tracking performance and strong robustness of disturbance rejection.

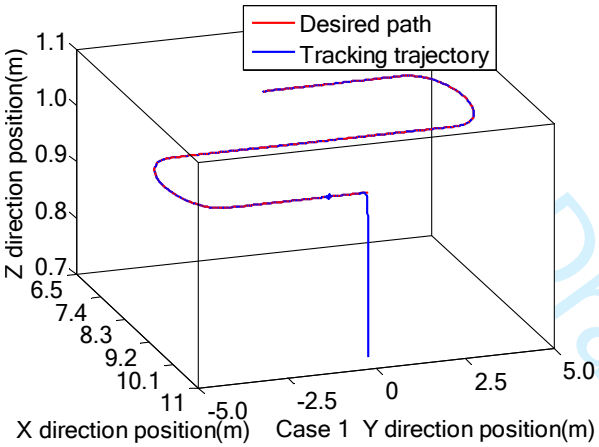

Fig. 7. Trajectories (case 1)

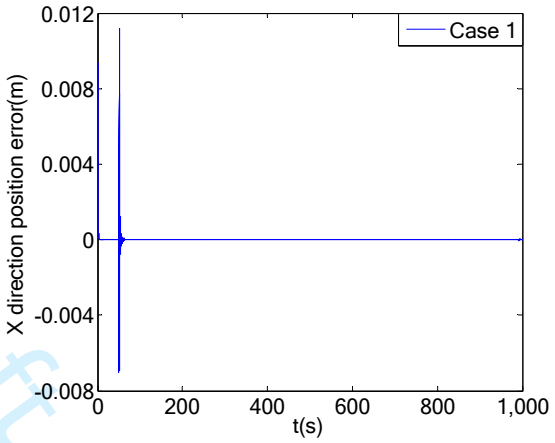

Fig. 8. X direction position error (case 1)

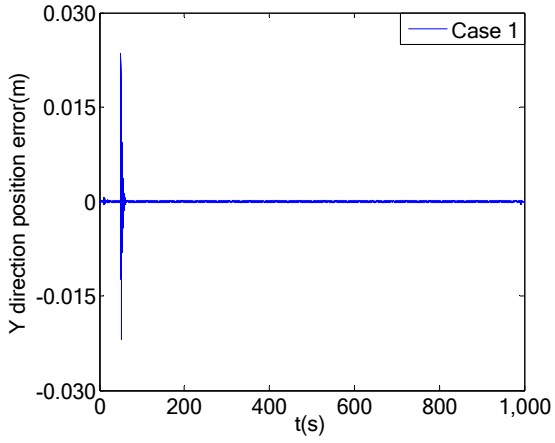

Fig. 9. Y direction position error (case 1)

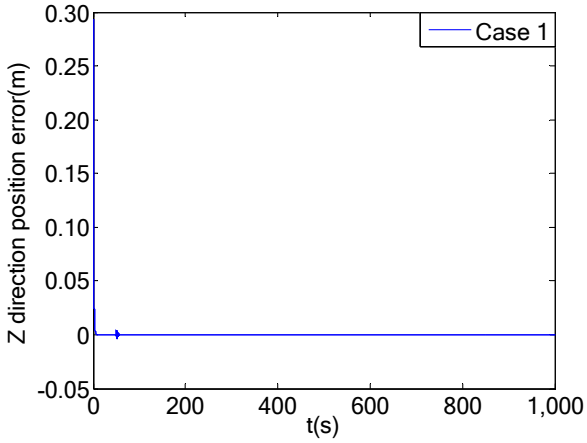

Fig. 10. Z direction position error (case

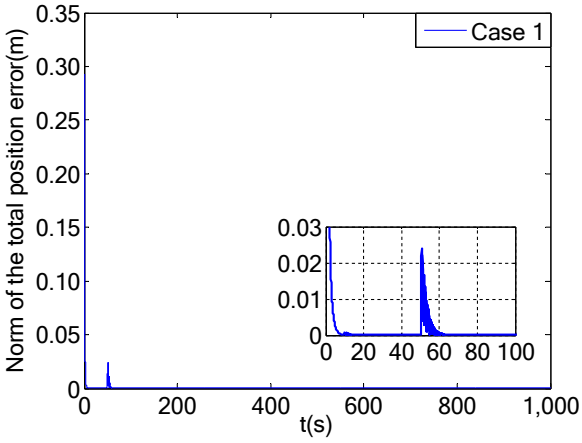

Fig. 11. Norm of total position errors (case 1)

1)

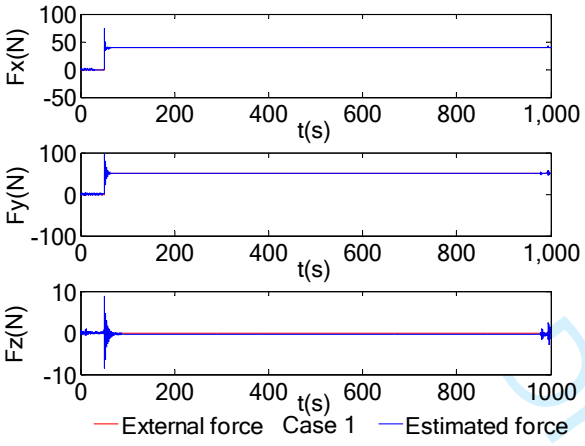

Fig. 12. Force and its estimation (case 1)

In Figs. 13-15, time trajectories of the manipulator end effector under three control schemes are represented throughout the whole tracking process. It can be observed that all of three schemes can guarantee high-precision tracking performance of the system, although some oscillations exist at certain periods. That is because both of the lumped disturbances and external force change suddenly at 50s, which produces slightly large position errors of the manipulator end effector but within reasonable limits.

Figure 16 shows the three position errors in X direction that can all converge to [-0.005, +0.005] m within 5 seconds for the initial phase. Afterwards, there is a little larger chattering of the position error the in case 2 as compared to case 3 and case 4. After t=50s, all of their position errors become much larger due to the sudden changes of the external factors. For

example, the maximum position error in case 2 varies from less 0.005m to over 0.06 m within few seconds. Owing to the compensation for the external effects, after about 20 seconds the position error in case 4 shows much faster and smoother convergence than those in other two cases. Finally, their steady-state position errors in X direction can all reach the range of a [-0.003, +0.003] m. Three position errors in Y direction are presented in Fig. 17, in which they can converge fast and reject the external interferences strongly, and finally achieve the steady response. Whereas, they are affected a little worse in contrast to those in Fig. 16.

Figure 18 indicates the Z direction position errors under three cases. The results show that they can even reach the range of [-0.10, +0.07] m, [-0.04, +0.03] m, and [-0.02, +0.02] m from 50s to 60s, respectively. After that the effects of the perturbations are gradually weakened thanks to the compensation of both AWNN and force estimation methods. Finally, all of their steady-state errors can achieve a small range of about [-0.005, +0.005] m. Three total position errors are depicted in Fig. 19. And, the fact is that for the initial phase the total position error in case 2 has much larger oscillations than other two cases. Then at about [50, 100] s this error in case 4 is affected the least by the external factors, and one in case 3 is less than that in case 2. Afterwards, all of them can converge fast and finally achieve the steady-state errors of [0, 0.005] m (see Fig. 19). Also, on the basis of Figs. 16-19, it can be observed that our proposed scheme in case 4 can provide much faster convergence, higher precision tracking performance and stronger disturbance rejection than other two cases.

Figures 20-22 illustrate the time responses of the external force and its estimation under three cases, respectively. Especially, at 50s all of their estimations vary abruptly, and their force estimation errors of both case 3 and 4 have less variation than that of case 2. After

about 50 seconds, their estimation errors can all become much smaller till within bounded regions in the end. Besides, the results of the averaged position errors, averaged total position error and averaged force estimation error are shown in Table 3. Among them, all of their four position errors have the decreasing trend from case 2 to case 3, and then to case 4. Moreover, the averaged force estimation error in case 2 shows a little larger than those in both case 3 and case 4, in which both of them have a few difference.

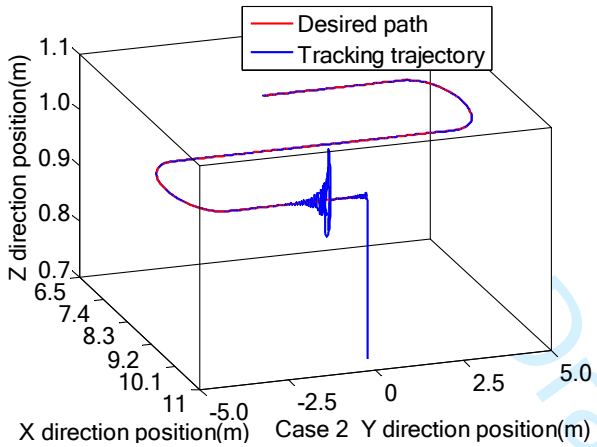

Fig. 13. Trajectories (case 2)

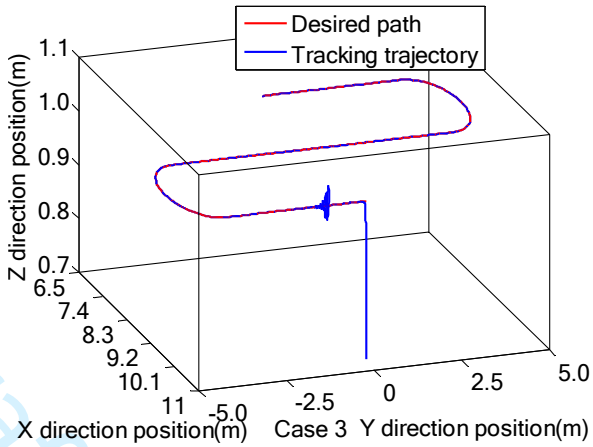

Fig. 14. Trajectories (case 3)

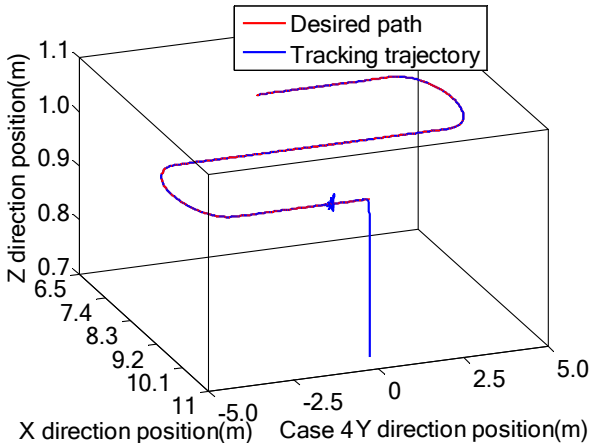

Fig. 15. Trajectories (case 4)

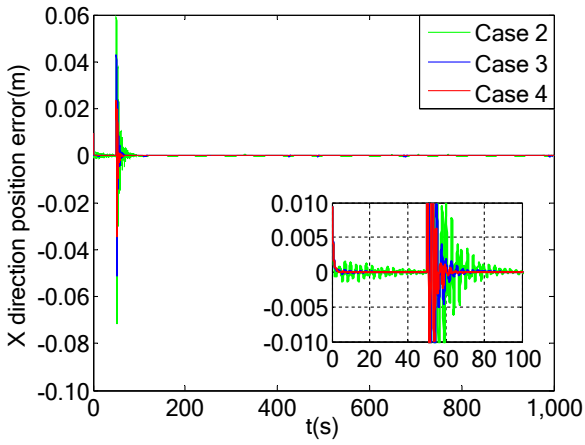

Fig. 16. X direction position errors (case 2-4)

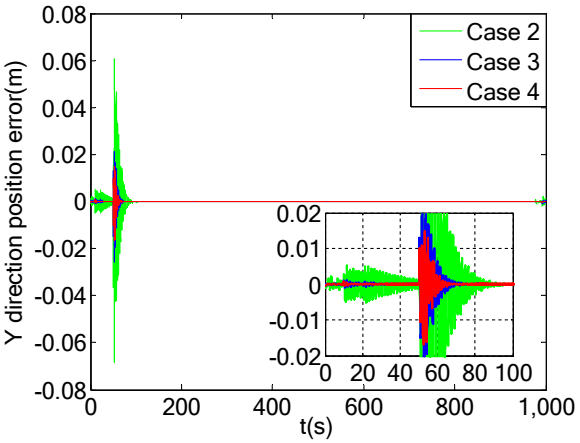

Fig. 17. Y direction position errors (case 2-4)

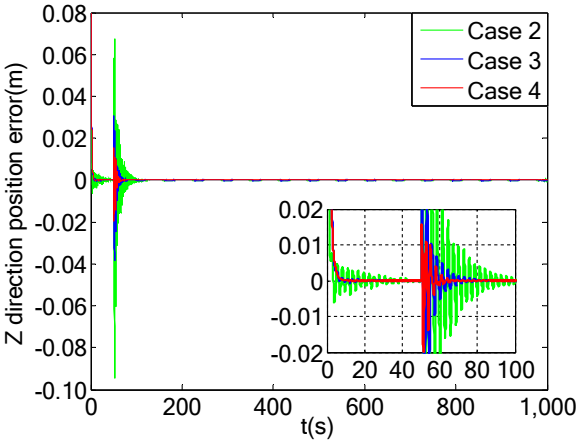

Fig. 18. Z direction position errors (case 2-4)

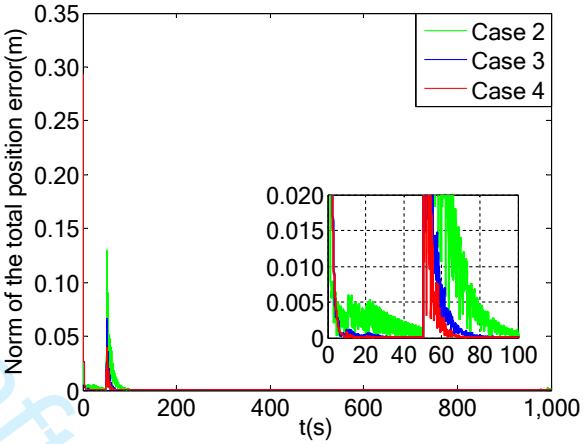

Fig. 19. Norm of total errors (case 2-4)

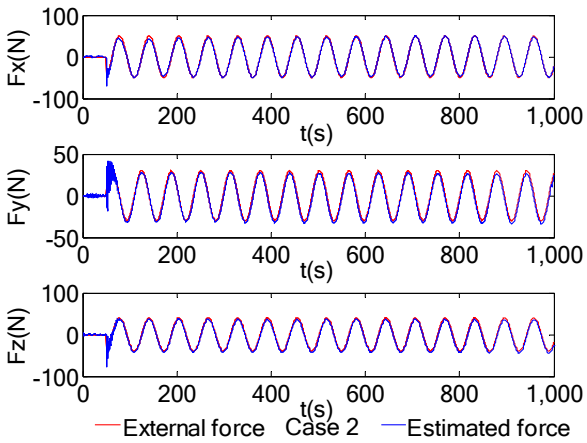

Fig. 20. Force and estimation (case 2)

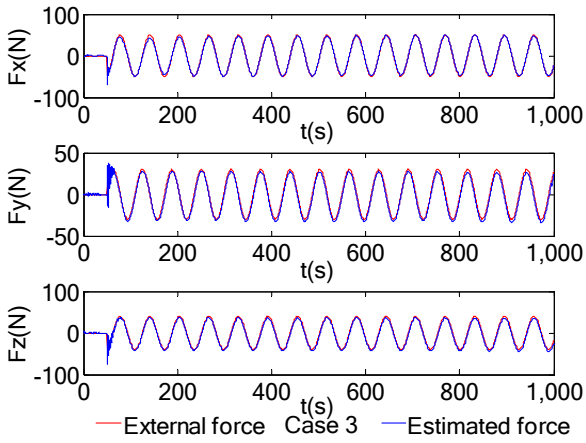

Fig. 21. Force and estimation (case 3)

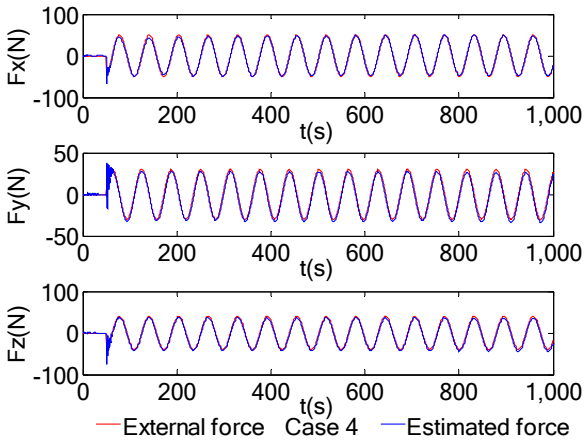

Fig. 22. Force and estimation (case 4)

For case 5, results of time responses for desired path and tracking trajectory, three position errors in X, Y, Z directions and their total position error, and the external force and its estimation are described in Figs. 23-28, respectively. It can be seen from Fig. 23 that the control system under such situation shows better tracking performance. Although all of three position errors (see Figs. 24-26) generate high chattering at about 50s due to the lumped disturbances and the external force, they can all achieve fast convergence and finally reach the range of about [-0.005, +0.005] m. In Fig. 27, the steady-state value of their total position error can keep within [0, 0.005] m in the final phase. Figure 28 shows larger component errors between the external force and its estimation than those in case 4 (see Fig. 22). Seen from Table 3, the values of their averaged position errors and averaged total position error in case 4 and case 5 have few differences. While the averaged force estimation error in case 5 increases more than two times larger as compared to that in case 4, these results are still within the allowable limits. That stems from the existing uncertainties of the gravitational and hydrodynamic terms in case 5.

In summary, those results conclude that the control system in case 4 and case 5 have

faster convergence, better tracking performance and stronger robustness of disturbance rejection, which validate the effectiveness of the proposed method.

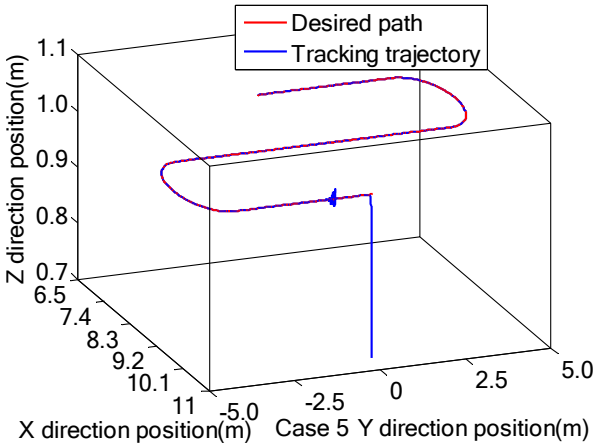

Fig. 23. Trajectories (case 5)

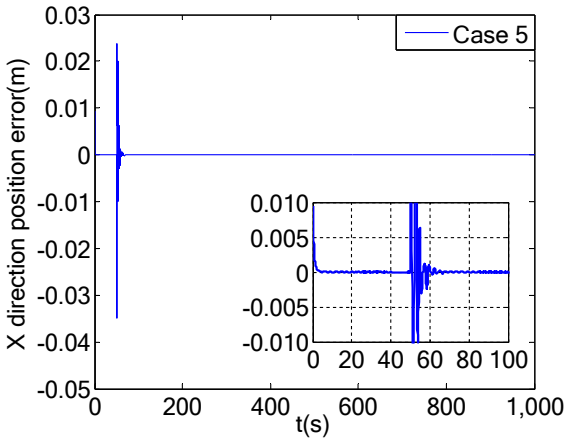

Fig. 24. X direction position error (case 5)

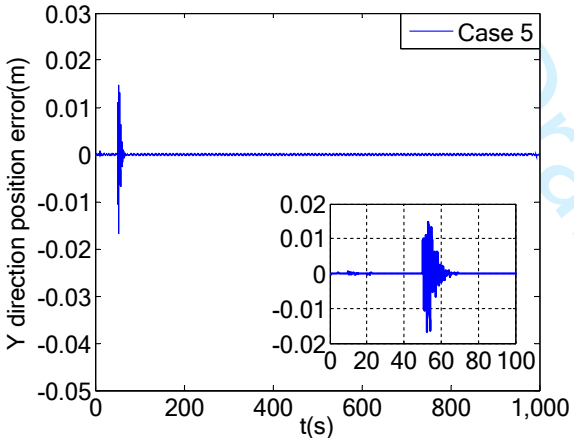

Fig. 25. Y direction position error (case 5)

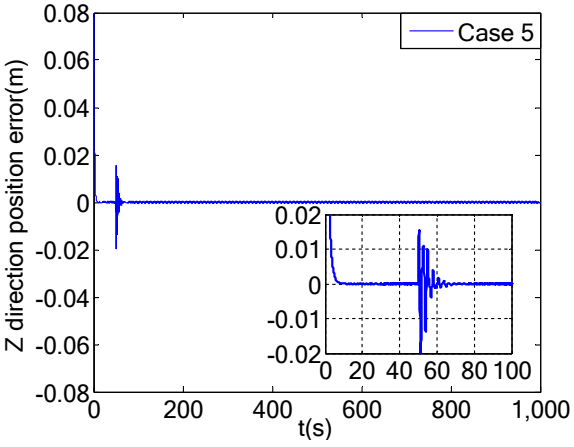

Fig. 26. Z direction position error (case 5)

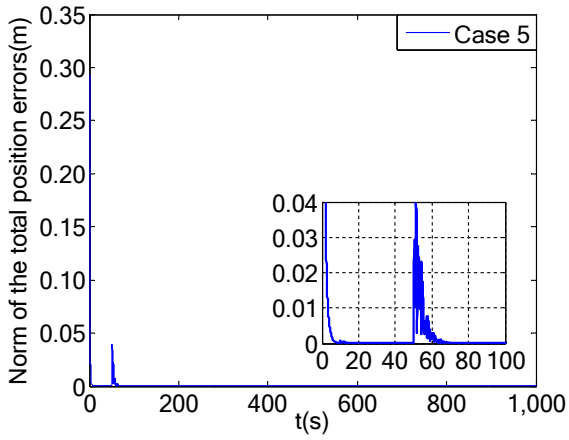

Fig. 27. Norm of total error (case 5)

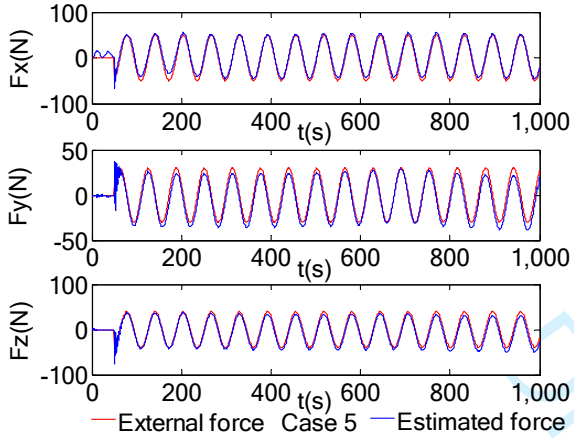

Fig. 28. Force and estimation (case 5)

Table 3. The averaged tracking errors of the system

Cases	E_x/m	E_y/m	E_z/m	E_t/m	E_f/N
Case 2	0.0027	0.0036	0.0074	0.0087	4.4228
Case 3	0.0018	0.0012	0.0069	0.0073	4.3417
Case 4	0.0012	7.5716e-04	0.0068	0.0069	4.3606
Case 5	0.0012	7.6055e-04	0.0068	0.0069	9.1740

5. Conclusion

In this paper, the AWNN-NTSMC strategy with force estimation is developed for the path tracking control of the underwater manipulator under the presence of the lumped disturbances, including parameter uncertainties and external disturbances. Based on the adaptive laws to adjust the network parameters online, the WNN scheme can effectively

estimate the lumped disturbances. In addition, the force estimation method is considered to attenuate the effects of external force exerted on the manipulator end effector. Also, a saturated function is used to replace the signum function to reduce the chattering phenomenon. Under the proposed AWNN-NTSMC scheme, the position tracking errors tend to zero asymptotically through the Lyapunov stability. To verify this, a six DOF underwater manipulator is advised to conduct the numerical simulation in five cases. In comparison with other schemes, faster convergence, higher-precision tracking performance and stronger robustness against disturbances, presented in the simulation results demonstrate the feasibility and effectiveness of the proposed controller.

Acknowledgement

This research is supported by the National Natural Science Foundation of China (No. 51979116), the HUST Interdisciplinary Innovation Team Project, the Innovation Foundation of Maritime Defense Technologies Innovation Center and the Fundamental Research Funds for the Central Universities, HUST: 2018JYCXJJ045, HUST: 2018KFYYXJJ012. The author(s) declared no potential conflicts of interest with respect to the research, authorship, and/or publication of this article.

References

Bhat, S.P., and Bernstein, D.S. 2005. Geometric homogeneity with applications to finite-time stability. Math. Control Signals Systems, **17**(2): 101-127. doi:10.1007/s00498-005-0151-x.

Chu, Y.D., and Fei, J.T. 2017. Dynamic global PID sliding control using neural compensator for active power filter. In Proceedings of the SICE Annual Conference, Kanazawa, Japan, 19-22 September 2017. pp. 1513-1517.

Danesh, M., Sheikholeslam, F., and Keshmiri, M. 2005. External force disturbance rejection in robotic arms: an adaptive approach. IEICE Trans. Fundamentals, **E88-A** (10): 2504 -2513. doi:10.1093/ietfec/e88-a.10.2504.

Dehghan, S.A.M., Danesh, M., Sheikholeslam, F., and Zekri, M. 2015. Adaptive force-environment estimator for manipulators based on adaptive wavelet neural network. Appl. Soft Comput. **28**: 527-540. doi:10.1016/j.asoc.2014.12.021.

Ellery, A., Kreisel, J., and Sommer, B. 2008. The case for robotic on-orbit servicing of spacecraft: spacecraft reliability is a myth. Acta Astronautica, **63**(5-6): 632-648. doi:10. 1016/j.actaastro.2008.01.042.

Gao, J., An, X.M., Proctor, A., and Bradley, C. 2017. Sliding mode adaptive neural network control for hybrid visual servoing of underwater vehicles. Ocean Eng. **142**: 666-675. doi: 10.1016/j.oceaneng.2017.07.015.

Hsu, C.F., Lin, C.M., and Lee, T.T. 2006. Wavelet adaptive backstepping control for a class of nonlinear systems. IEEE Trans. Neural Netw. **17**(5): 1175-1183. doi:10.1109/TNN.2006. 878122.

Jafarov, E.M., Parlakci, M.N.A., and Istefanopulos, Y. 2005. A new variable structure PID-controller design for robot manipulators. IEEE Trans. Control Syst. Technol. **13**(1): 122-130. doi:10.1109/TCST.2004.838558.

Jin, M.L., Kang, S.H., Chang, P.H., and Lee, J. 2017. Robust control of robot manipulators using inclusive and enhanced time delay control. IEEE/ASME Trans. Mechatron. **22**(5): 2141-2152. doi:10.1109/TMECH.2017.2718108.

Katsura, S., Matsumoto, Y., and Ohnishi, K. 2006. Analysis and experimental validation of force bandwidth for force control. IEEE Trans. Ind. Electron. **53**(3): 922-928. doi:10. 1109/TIE.2006.874262.

Kawamura, S., Iwamoto, Y., Minamoto, H., Kamigaki, T., Taniyama, Y., and Kawamura, H. 2009. Structural design optimization for a two-link robot to suppress undesirable vibration. Journal of Advanced Mechanical Design, Systems, and Manufacturing, **3**(4): 289-298. doi:10.1299/jamdsm.3.289.

Lin, F.J., Wai, R.J., and Chen, H.P. 1998. A PM synchronous servo motor drive with an on-line trained fuzzy neural network controller. IEEE Trans. on Energy Convers. **13**(4): 319-325. doi:10.1109/60.736317.

Lin, C.K. 2006. Nonsingular terminal sliding mode control of robot manipulators using fuzzy wavelet networks. IEEE Trans. Fuzzy Syst. **14**(6): 849-859. doi:10.1109/TFUZZ.2006. 879982.

Mohan, S., and Kim, J. 2015. Robust PID control for position tracking of an underwater manipulator. In Proceedings of the IEEE International Conference on Advanced Intelligent Mechatronics (AIM), Busan, Korea, 7-11 July 2015. pp. 1707-1712.

Mobayen, S. 2015. An adaptive fast terminal sliding mode control combined with global sliding mode scheme for tracking control of uncertain nonlinear third-order systems. Nonlinear Dyn. **82**(1-2): 599-610. doi:10.1007/s11071-015-2180-4.

Murakami, T., Nakamura, R., Yu, F.M., and Ohnishi, K. 1993. Force sensorless impedance control by disturbance observer. In Proceedings of the Power Conversion Conference, Yokohama, Japan, 19-21 April 1993. pp. 352-357.

Ngo, V.T., and Liu, Y.C. 2018. Object transportation using networked mobile manipulators without force/torque sensors. In Proceedings of the International Automatic Control Conference (CACS), Taoyuan, Taiwan, 4-7 November 2018. pp.1-6.

Oussar, Y., Rivals, I., Personnaz, L., and Dreyfus, G. 1998. Training wavelet networks for nonlinear dynamic input-output modeling. Neurocomputing, **20**(1-3): 173-188. doi:10.1016/S0925-2312(98)00010-1.

Qiao, L., and Zhang, W.D. 2019. Double-loop integral terminal sliding mode tracking control for UUVs with adaptive dynamic compensation of uncertainties and disturbances. IEEE J. Ocean. Eng. **44**(1): 29-53. doi:10.1109/JOE.2017.2777638.

Qiao, L., and Zhang, W.D. 2020. Trajectory tracking control of AUVs via adaptive fast nonsingular integral terminal sliding mode control. IEEE Trans. Ind. Informat. **16**(2): 1248-1258. doi:10.1109/TII.2019.2949007.

Rubio, J.J. 2012. Modified optimal control with a backpropagation network for robotic arms. IET Control Theory Appl. **6**(14): 2216-2225. doi:10.1049/ iet-cta.2011.0322.

Smith, A.C., Mobasser, F., and Zaad, K.H. 2006. Neural-network-based contact force observers for haptic applications. IEEE Trans. Robot. **22**(6): 1163-1175. doi:10.1109/ TRO.2006.882923.

Song, H.T., and Zhang, T. 2016. Fast robust integrated guidance and control design of interceptiors. IEEE Trans. Control Syst. Technol. **24**(1): 349-356. doi:10.1109/TCST.2015.2431641.

Vijay, M., and Jena, D. 2018. Backstepping terminal sliding mode control of robot manipulator using radial basis functional neural networks. Computers and Electrical Engineering, **67**: 690-707. doi:10.1016/j.compeleceng.2017.11.007.

Wai, R.J., and Chen, P.C. 2004. Intelligent tracking control for robot manipulator including actuator dynamics via TSK-type fuzzy neural network. IEEE Trans. Fuzzy Syst. **12**(4): 552-559. doi:10.1109/TFUZZ.2004.832531.

Wai, R.J., and Muthusamy, R. 2013. Fuzzy-neural-network inherited sliding-mode control for robot manipulator including actuator dynamics. IEEE Trans. Neural Netw. Learn. Syst. **24**(2): 274-287. doi:10.1109/TNNLS.2012.2228230.

Wang, Y.Y., Gu, L.Y., Xu, Y.H., and Cao, X.X. 2016. Practical tracking control of robot manipulators with continuous fractional-order nonsingular terminal sliding mode. IEEE Trans. Ind. Electron. **63**(10): 6194-6204. doi:10.1109/TIE.2016.2569454.

Wang, Y.Y., Zhu, K.W., Chen, B., and Jin, M.L. 2019a. Model-free continuous nonsingular fast terminal sliding mode control for cable-driven manipulators. ISA Trans. **98**: 483-495. doi:10.1016/j.isatra.2019.08.046.

Wang, Y.Y., Yan, F., Chen, J.W., Ju, F., and Chen, B. 2019b. A new adaptive time-delay control scheme for cable-driven manipulators. IEEE Trans. Ind. Informat. **15**(6): 3469-3481. doi:10.1109/TII.2018.2876605.

Wang, Y.Y., Yan, F., Zhu, K.W., Chen, B., and Wu, H.T. 2019c. A new practical robust control of cable-driven manipulators using time-delay estimation. Int. J. Robust Nonlinear Control, **29**(11): 3405-3425. doi:10.1002/rnc.4566.

Wang, Y.Y., Liu, L.F., Wang, D., Ju, F., and Chen, B. 2020. Time-delay control using a novel nonlinear adaptive law for accurate trajectory tracking of cable-driven robots. IEEE Trans. Ind. Informat. **16**(8): 5234-5243. doi:10.1109/TII.2019.2951741.

Wei, S.N., Wang, Y.N., and Zuo, Y. 2012. Wavelet neural networks robust control of farm transmission line deicing robot manipulators. Computer Standards & Interfaces, **34**(3): 327-333. doi:10.1016/j.csi.2011.11.001.

Appendices

1) The design of the control law in the NTSMC scheme

Combining with eqs. (1), (11) and (12), we can get to the following expressions:

$$\begin{aligned}\mathbf{M}\dot{\boldsymbol{s}} &= \mathbf{M}\ddot{\boldsymbol{\theta}} - \mathbf{M}\ddot{\boldsymbol{\theta}}_r \\ &= -\mathbf{C}(\boldsymbol{\theta},\dot{\boldsymbol{\theta}})\dot{\boldsymbol{\theta}} - \boldsymbol{G}(\boldsymbol{\theta}) - \boldsymbol{\tau}_h - \boldsymbol{\tau}_d + \boldsymbol{\tau} + \mathbf{J}^{\mathrm{T}}\boldsymbol{F}_{ext} - \mathbf{M}\ddot{\boldsymbol{\theta}}_r \\ &= -\mathbf{M}\ddot{\boldsymbol{\theta}}_r - \mathbf{C}(\boldsymbol{\theta},\dot{\boldsymbol{\theta}})\dot{\boldsymbol{\theta}} - \boldsymbol{G}(\boldsymbol{\theta}) - \boldsymbol{\tau}_h - \boldsymbol{\tau}_d + \boldsymbol{\tau} + \mathbf{J}^{\mathrm{T}}\boldsymbol{F}\end{aligned} \tag{A1}$$

$$\mathbf{M}\dot{\boldsymbol{s}} + \mathbf{C}\boldsymbol{s} = -\mathbf{M}\ddot{\boldsymbol{\theta}}_r - \mathbf{C}(\boldsymbol{\theta},\dot{\boldsymbol{\theta}})\dot{\boldsymbol{\theta}}_r - \boldsymbol{G}(\boldsymbol{\theta}) - \boldsymbol{\tau}_h - \boldsymbol{\tau}_d + \boldsymbol{\tau} + \mathbf{J}^{\mathrm{T}}\boldsymbol{F} \tag{A2}$$

Consider that $\hat{\mathbf{M}}(\boldsymbol{\theta})$, $\hat{\mathbf{C}}(\boldsymbol{\theta},\dot{\boldsymbol{\theta}})$, $\hat{\boldsymbol{G}}(\boldsymbol{\theta})$ and $\hat{\boldsymbol{\tau}}_h$ are nominal model parameters satisfying $\Delta\mathbf{M}(\boldsymbol{\theta}) = \mathbf{M}(\boldsymbol{\theta}) - \hat{\mathbf{M}}(\boldsymbol{\theta})$, $\Delta\mathbf{C}(\boldsymbol{\theta},\dot{\boldsymbol{\theta}}) = \mathbf{C}(\boldsymbol{\theta},\dot{\boldsymbol{\theta}}) - \hat{\mathbf{C}}(\boldsymbol{\theta},\dot{\boldsymbol{\theta}})$, $\Delta\boldsymbol{G}(\boldsymbol{\theta}) = \boldsymbol{G}(\boldsymbol{\theta}) - \hat{\boldsymbol{G}}(\boldsymbol{\theta})$, $\Delta\boldsymbol{\tau}_h = \boldsymbol{\tau}_h - \hat{\boldsymbol{\tau}}_h$. Then, eq. (A2) can be rewritten as follows,

$$\mathbf{M}\dot{\boldsymbol{s}} + \mathbf{C}\boldsymbol{s} = -\hat{\mathbf{M}}\ddot{\boldsymbol{\theta}}_r - \hat{\mathbf{C}}(\boldsymbol{\theta},\dot{\boldsymbol{\theta}})\dot{\boldsymbol{\theta}}_r - \hat{\boldsymbol{G}}(\boldsymbol{\theta}) - \hat{\boldsymbol{\tau}}_h + \boldsymbol{f} + \boldsymbol{\tau} + \mathbf{J}^{\mathrm{T}}\boldsymbol{F}_{ext} \tag{A3}$$

where the lumped disturbance vector $\boldsymbol{f} = -\Delta\mathbf{M}(\boldsymbol{\theta})\ddot{\boldsymbol{\theta}}_r - \Delta\mathbf{C}(\boldsymbol{\theta},\dot{\boldsymbol{\theta}})\dot{\boldsymbol{\theta}}_r - \Delta\boldsymbol{G}(\boldsymbol{\theta}) - \Delta\boldsymbol{\tau}_h - \boldsymbol{\tau}_d$ that is bounded as $\| \boldsymbol{f} \|_1 \le L_f$. Having chosen the modified NTSMC variable in eq. (7), the next step should be the design of the control law in such a way that the following condition called reaching condition is met:

$$\boldsymbol{s}^{\mathrm{T}} \cdot \dot{\boldsymbol{s}} < 0 \tag{A4}$$

and $\dot{\boldsymbol{s}}$ is typically chosen as the following reaching law:

$$\dot{\boldsymbol{s}} = -\varepsilon_r \cdot \mathrm{sign}(\boldsymbol{s}) \tag{A5}$$

$$\dot{\boldsymbol{s}} = -\varepsilon_r \cdot \mathrm{sign}(\boldsymbol{s}) - \mathbf{K}_r \cdot \boldsymbol{s} \tag{A6}$$

Under the case of $\hat{\boldsymbol{F}}$ being defined as the estimation of the external force $\boldsymbol{F}_{ext}$, eqs. (A3) and (A5) have been considered to determine the control law that is designed as eq. (13).

2) The design of the control law in the AWNN-NTSMC scheme

In this situation that the boundness of the lumped disturbance vector $\boldsymbol{f}$ is assumed to be unknown, $\boldsymbol{f}$ will be approached by the WNN scheme. Thus a similar control law as given by eq. (24) can be designed according to the reaching law in eq. (A6).